PHYSICAL REVIEW E, VOLUME 64, 025201(R)

Tunneling mechanism due to chaos in a complex phase space

T. Onishi,[1] A. Shudo,[1] K. S. Ikeda,[2] and K. Takahashi[3]
[1]*Department of Physics, Tokyo Metropolitan University, Minami-Ohsawa, Hachioji 192-0397, Japan*
[2]*Faculty of Science and Engineering, Ritsumeikan University, Noji-cho 1916, Kusatsu 525-0055, Japan*
[3]*The Physics Laboratories, Kyushu Institute of Technology, Kawazu 680-4, Iizuka 820-8502, Japan*
(Received 24 July 2000; revised manuscript received 16 April 2001; published 17 July 2001)

We have revealed that the barrier-tunneling process in nonintegrable systems is strongly linked to chaos in complex phase space by investigating a simple scattering map model. The semiclassical wave function reproduces complicated features of tunneling perfectly and it enables us to solve all the reasons why those features appear in spite of absence of chaos on the real plane. Multigeneration structure of manifolds, which is the manifestation of complex-domain homoclinic entanglement created by complexified classical dynamics, allows a symbolic coding and it is used as a guiding principle to extract dominant complex trajectories from all the semiclassical candidates.

DOI: 10.1103/PhysRevE.64.025201 PACS number(s): 05.45.Mt, 03.65.Ge, 03.65.Sq, 05.10.−a

Tunneling phenomenon is peculiar to quantum mechanics and no counterparts exist in classical mechanics. Features of tunneling are nevertheless strongly influenced by the underlying classical dynamics [1–6]. In particular, chaotic features appearing in tunneling have been paid attention to in connection with *real-domain chaos* [2–4].

A promising approach to see the connection of these two opposite concepts is to carry out the complex semiclassical analysis, which allows us to describe and interpret the tunneling phenomenon in terms of complex classical trajectories [7]. It has been shown that the complex semiclassical theory can successfully be applied even in classically chaotic systems and the origin of characteristic structures of the wave function inherent in chaotic systems is explained by the complex classical dynamics [5]. A significant role of almost real-domain homoclinic trajectories in the energy barrier tunneling has been pointed out based on the trace formula approach [8]. Recently, it is found that fringed pattern appears in the wave function of the two-dimensional barrier tunneling problem as a result of interference between oscillatory Lagrangian manifold [9]. They have shown a detailed scenario describing how such interference emerges in accordance with the divergent movement of singularities on the complex t-plane.

In the present Rapid Communication, we shall report the strong connection between the barrier-tunneling process in nonintegrable systems and the *chaos in complex phase space* by analyzing a simple scattering map model. In particular, it will be shown that even though the real-domain classical dynamics exhibits no chaos, i.e., null topological entropy, complex-domain chaos can make tunneling process complicated. Moreover, our present analysis suggests that chaotic tunneling can be understood in a unified manner from the viewpoint of complex-domain chaos not only in case of dynamical but also energy-barrier tunneling processes.

We first introduce a scattering map model which is described by the following Hamiltonian

$$\mathcal{H}(q,p,t)=T(p)+V(q)\sum_n \delta(t-n), \tag{1a}$$

$$T(p)=p^2/2, \quad V(q)=k\exp(-\gamma q^2) \quad (k,\gamma>0). \tag{1b}$$

A set of classical equations of motion is given as $(q_{j+1},p_{j+1})=[q_j+T'(p_j),p_j-V'(q_{j+1})]$, where prime denotes a differentiation with respect to the corresponding argument. Note that the real-valued dynamics of our scattering map does not create chaos in contrast to the maps defined on the bounded phase space. This is because the system has only single periodic orbit, $(q,p)=(0,0)$, and thus the topological entropy of the system is null. As shown in the inset of Fig. 1, the stable and unstable manifolds of the fixed point (0,0), $\mathcal{W}^s(0,0)$ and $\mathcal{W}^u(0,0)$, oscillate without creating homoclinic or heteroclinic intersections. Any manifold initially put on the real plane is fully stretched but not folded perfectly so that it leaves away to infinity along $\mathcal{W}^u(0,0)$.

An incident wave packet is put in the asymptotic region. The initial kinetic energy is given far less than the potential barrier located around the origin. The form of initial wave packet is given by

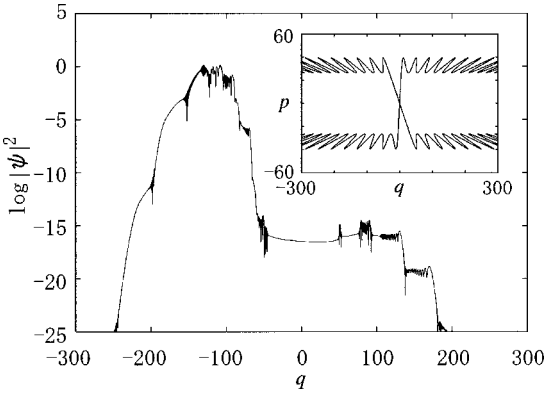

FIG. 1. $|\langle q|U^n|\Psi\rangle|^2$ for $n=10$ calculated quantum-mechanically ($\hbar=1$, $\sigma=10$, $k=500,\gamma=0.005$, $q_\alpha=-123$, $p_\alpha=23$). An incident wave packet is set in the side of $q<0$. The center of mass has been already reflected by the potential barrier at this time step. (Inset) $\mathcal{W}^s(0,0)$ and $\mathcal{W}^u(0,0)$ merely oscillating without homoclinic entanglement.

$$\langle q|\Psi\rangle = \mathcal{C}\exp\left[-\frac{(q-q_\alpha)^2}{2\hbar\sigma^2}\right]\exp\left[-i\frac{p_\alpha(q_\alpha-2q)}{2\hbar}\right], \quad (2)$$

where $\mathcal{C}$ is the normalization constant, σ is the squeezing parameter, and q_α, p_α are configuration and momentum of the center of mass, respectively.

$|\langle q|U^n|\Psi\rangle|^2$ for $n=10$ is shown in Fig. 1, where U denotes the unitary operator of one-step quantum propagation. Although the mean energy of the wave packet is less than the barrier height, we can observe various structures such as crossover of amplitude, existence of plateau regions, erratic oscillation on them, cliffs and so on. Similar structures are also found in case of dynamical tunneling in the presence of chaos [5], and we hereafter call such characteristic structures ''plateau-cliff structure'' as a representative of typical features which are completely absent in one-dimensional tunneling. However, an essential difference of the present situation from the previous one is that the plateau-cliff structure in the scattering model emerges under the situation where the real-valued classical dynamics creates no chaos.

In order to carry out complex semiclassical analysis, we first prepare a pair of new canonical variables as $Q\equiv(q-ip\sigma^2)/(\sqrt{2}\sigma)$, $P\equiv(p-iq\sigma^{-2})/(\sqrt{2}\sigma^{-1})$, and some notations as $Q_0\equiv Q(q_0,p_0)$, $P_0\equiv P(q_0,p_0)$, $Q_\alpha\equiv Q(q_\alpha,p_\alpha)$, $P_\alpha\equiv P(q_\alpha,p_\alpha)$. The n-step quantum propagator is represented as the n-fold multiple integral, and the saddle point evaluation is applied to yield the classical equations. Semiclassical Van Vleck's formula for n-step wave function takes a form as

$$\langle q_n|U^n|\Psi\rangle \approx \mathcal{A}\sum_{cl.orb.}\left|\frac{\partial^2 W}{\partial q_n \partial P_0}\right|^{1/2}\exp\frac{i}{\hbar}\left[\mathcal{S}-\frac{\phi}{2}\right], \quad (3)$$

where the sum is over complex classical orbits satisfying the boundary condition, $\mathrm{Im}\, q_n=0$, which is necessary since we here observe our wave function as a function of q_n. $\mathcal{A}$ denotes the normalization factor, and $\mathcal{S},\phi$ are the action and the Maslov index of each contributing orbit respectively. W is the generating function which gives canonical transformations such that $\partial W/\partial q_n = p_n$, $\partial W/\partial P_0 = -Q_0$.

In order to represent the complex orbits which can contribute to the semiclassical propagator (3), we introduce a variable, $\Delta Q_0 \equiv Q_0 - Q_\alpha$. Using ΔQ_0 the contributing orbits in Eq. (3) are represented as a set of initial conditions $\mathcal{M}_n \equiv \{\Delta Q_0 | \Delta Q_0 \in \mathbf{C},\ \mathrm{Im}\, q_n(Q_\alpha+\Delta Q_0, P_\alpha)=0\}$.

A typical pattern of the $\mathcal{M}_n$-set is shown in Fig. 2(a). Each string, which we call the branch hereafter, represents an individual classical orbit appearing in the semiclassical sum (3) and a single string covers the whole range $(-\infty,+\infty)$ of the final q_n.

Though the morphology of the set is quite elusive, when sufficiently blowing up any local area with lots of branches accumulated, one can find the self-similar structure schematically demonstrated in Fig. 2(b). At the center, a chain-shaped structure is developed in the horizontal direction. A sequence of chains with finer scale are arranged in both sides of the previous chain, and does the same around any of those smaller chains, and so on. Then it may be natural to assign a

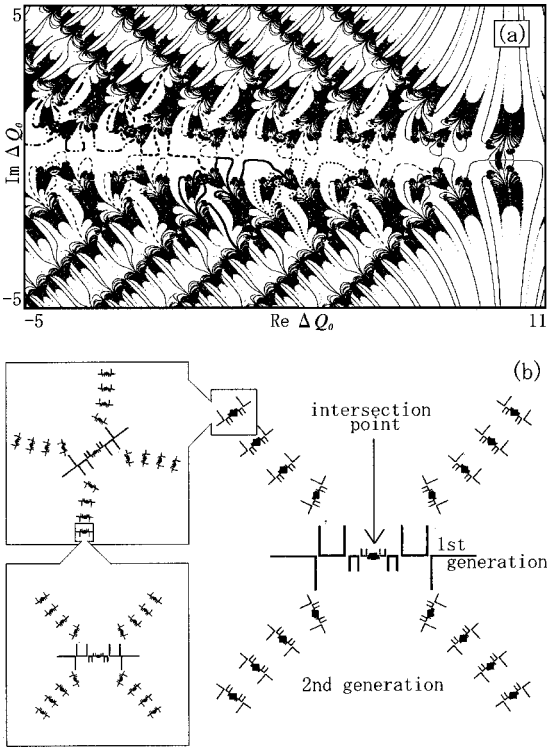

FIG. 2. (a) $\mathcal{M}_n$-set for $n=10$. Those branches which we finally take into account for the reproduction of the wave function are represented by the line styles such as dash, bold dash, bold solid, bold dot, bold dashed dot and bold dashed dot dot. Each line style corresponds to the one in Fig. 5. (b) Schematic representation for MGS. Blown-up figures of the second and third generations display the self similarity of MGS. Solid squares represent the intersection points with $\mathcal{W}^s(0,0)$.

notion of the *generation* to each chain as shown in the figure. Higher generations sprout from lower generations almost vertically, and we call these self-similar configurations the multigeneration structure (MGS).

We can discuss significant branches embedded in the hierarchical structure, which determine the semiclassical wave function (3). The amplitude of an individual contribution in the semiclassical sum is almost governed by $\mathrm{Im}\,\mathcal{S}$, an imaginary action, which implies that the orbit whose imaginary part is the smallest survives as the final semiclassical contribution. Furthermore, the amount of $\mathrm{Im}\,\mathcal{S}$ is roughly estimated by how deep each trajectory passes through the complex domain. This means that the history of each trajectory in complex domain is a primary factor concerning its weight in the semiclassical sum. It implies that the semiclassical wave function could not be reproduced until one finds how those orbits with the smallest imaginary actions behave, since it is almost impossible to extract significant trajectories out of a huge number of branches without any guiding principle.

To this end, we begin with the precise definition of MGS, which is given by considering the *stable and unstable manifolds in complex phase space*, in particular analytical continuation of the stable manifold $\mathcal{W}^s(0,0)$. In order to connect MGS with $\mathcal{W}^s(0,0)$ in complex space, we first introduce the normalized coordinate on $\mathcal{W}^s(0,0)$. Let Φ be the conjugation

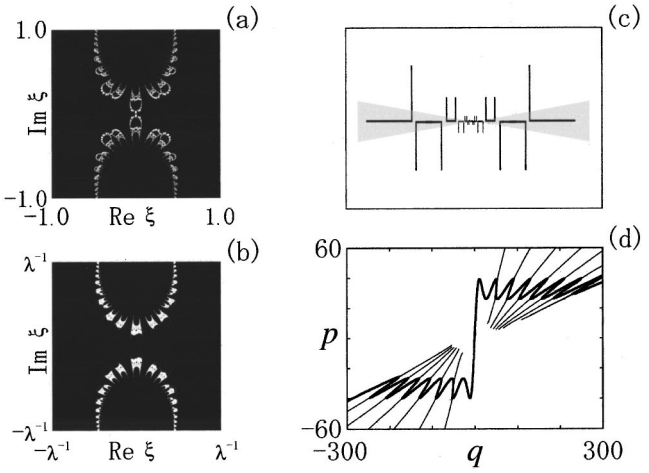

FIG. 3. (a) The intersection points belonging to the 1st, 2nd, or 3rd generation plotted on $\mathcal{W}^s(0,0)$. (b) Magnification of (a), displaying the 1st and 2nd generations. (c) Chain-shaped manifolds in the $\mathcal{M}_n$-set drawn schematically. (d) The final strings of those displayed in (c) after ten iterations of our map projected in real phase space. The hatched part in (c) develops to the bold curves, which almost coincide with the real-domain unstable manifold, $\mathcal{W}^u(0,0)\cap\mathbf{R}^2$.

map from $\mathbf{C}$ to $\mathcal{W}^s(0,0)$, satisfying the relation $\tilde{\mathcal{F}}(\xi) \equiv(\Phi^{-1})(\mathcal{F})\Phi(\xi)=\lambda^{-1}\xi$, where λ denotes the largest eigenvalue with respect to the saddle point (0,0) [10].

The normalized coordinate ξ is used in Figs. 3(a) and 3(b) to represent the intersection between $\mathcal{W}^s(0,0)$ and $\mathcal{I}$, the initial value plane consisting of the whole (q,p)'s corresponding to $\{\Delta Q_0|\Delta Q_0\in\mathbf{C}\}$. Comparing both figures, one can recognize the intersection pattern has self-similarity. The intersection between $\mathcal{W}^u(0,0)$ and $\mathcal{W}^s(0,0)$ shows almost the same self-similar pattern, which implies the *homoclinic entanglement* of the stable manifold in complex phase space [11]. This means that null topological entropy in the real domain does not exclude existence of chaos in the complex domain.

The generation can be assigned to each point on $\mathcal{I}\cap\mathcal{W}^s(0,0)$. Suppose r be the minimum distance on ξ-plane from (0,0) to intersection points $\Phi^{-1}[\mathcal{I}\cap\mathcal{W}^s(0,0)]$, and let $D\equiv\{\xi\in\mathbf{C}||\xi|\leqslant r\}$. Here the normalized coordinate plane is decomposed into disjointed annuli as

$$\tilde{\mathcal{F}}^m[D\setminus\tilde{\mathcal{F}}(D)]\cap\tilde{\mathcal{F}}^n[D\setminus\tilde{\mathcal{F}}(D)]=\phi \quad (m\neq n), \tag{4}$$

$$\bigsqcup_{n\in\mathbf{Z}}\tilde{\mathcal{F}}^n[D\setminus\tilde{\mathcal{F}}(D)]=\mathbf{C}\setminus\{0\}. \tag{5}$$

Then each annulus $\tilde{\mathcal{F}}^n[D\setminus\tilde{\mathcal{F}}(D)]$ plays a role specifying the individual generation. More precisely, if a point of $\mathcal{I}\cap\mathcal{W}^s(0,0)$ is contained in $\Phi\{\tilde{\mathcal{F}}^{-n}[D\setminus\tilde{\mathcal{F}}(D)]\}$, we say the point belongs to the nth generation.

Next we show that each point of $\mathcal{I}\cap\mathcal{W}^s(0,0)$ can be associated with a single chain structure on the $\mathcal{M}_n$-set, which is shown as the hatched zone in Fig. 3(c). The final strings of those displayed in the figure after ten iterations of our map are projected in real phase space in Fig. 3(d). The hatched part in Fig. 3(c) develops to the bold curves in Fig. 3(d), which almost coincide with the real-domain unstable manifold, $\mathcal{W}^u(0,0)\cap\mathbf{R}^2$.

This behavior is not limited to a particular chain-shaped structure, but every chain structure in the $\mathcal{M}_n$-set becomes close to $\mathcal{W}^u(0,0)\cap\mathbf{R}^2$. Chain-shaped structure is always created around each point of $\mathcal{I}\cap\mathcal{W}^s(0,0)$, the reason of which can be explained by describing the process of time evolution of a tiny domain containing a point of $\mathcal{I}\cap\mathcal{W}^s(0,0)$. Such a domain is guided to the real phase space by $\mathcal{W}^s(0,0)$ and then smeared over $\mathcal{W}^u(0,0)$. Details will be reported in Ref. [11]. In this way, we can find one-to-one relation between a single chain structure in the $\mathcal{M}_n$-set and an intersection point of $\mathcal{I}\cap\mathcal{W}^s(0,0)$. Since, as explained above, the latter forms the self-similar or generation structure reflecting the homoclinic entanglement of the stable manifold, MGS of the $\mathcal{M}_n$-set is controlled by that of the stable manifold in complex phase space.

Since we have defined the generation in such a way, the orbits belonging to higher generations usually gain larger $\mathrm{Im}\,\mathcal{S}$, since, taking roundabout ways in the complex chaotic region, they approach the origin later than those of lower generations. In order to extract significant trajectories out of them, it is essential to use symbolic dynamics in complex phase space.

In the present case, a nice symbolic space can be organized as the union of a single-element set $\{O\}$ and a direct product of the sign of $\mathrm{Re}\,q$, $\mathrm{Im}\,q$, and a multiplicity index $\nu\in\mathbf{N}$. The symbol ''O'' describes monotonic convergence to the origin (0,0), and the index ν appears as a reflection of the transcendental property of the potential function such that our initial-value problem has infinite number of solutions. Since frequent flipping of the sign or large modulus of q-component, which is represented as large ν, results in large imaginary actions, our final principle turns out to extract the sequences of symbols out of MGS which represent those orbits with no sign flipping and minimal q-components with $\nu=1$. It considerably reduces our task in searching significant complex orbits only to linear dependence of the time step, which otherwise exponentially diverges. More detailed explanations to construct symbolic dynamics in the complex-domain chaos will be reported elsewhere [11]. In particular, a complex Hénon map is analyzed to elucidate the relation between the MGS and Julia set [12].

Figure 4 displays the behaviors of intersection points in MGS as a function of time, together with the coding sequences. Figure 4(a) shows a typical behavior such that both $\mathrm{Re}\,q$ and $\mathrm{Im}\,q$ oscillate in an erratic manner for some initial time steps and eventually approach the origin. Figure 4(b) shows such an orbit trapped by complex period-2 orbits as evidence of regular behavior embedded in MGS. Such itinerating or oscillating complex orbits contribute in principle, however, their amplitudes are much smaller than those of orbits with $\mathrm{Re}\,q$ and $\mathrm{Im}\,q$ decreasing monotonically to zero, as shown in Fig. 4(c).

The semiclassical wave function evaluated finally takes the form in Fig. 5. The agreement with the quantal one

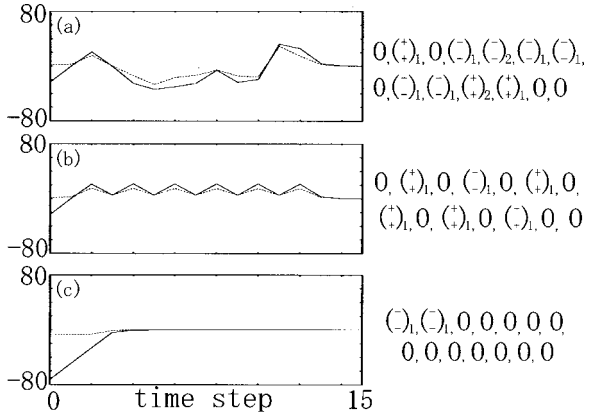

FIG. 4. Behaviors of intersection points in MGS. Solid lines as Re q, and broken lines as Im q. The sequences of symbols coding them also attached. These are the trajectories (a) showing stochastic motions, (b) temporarily attracted by a complex period-2 orbit, and (c) approaching real phase space monotonically.

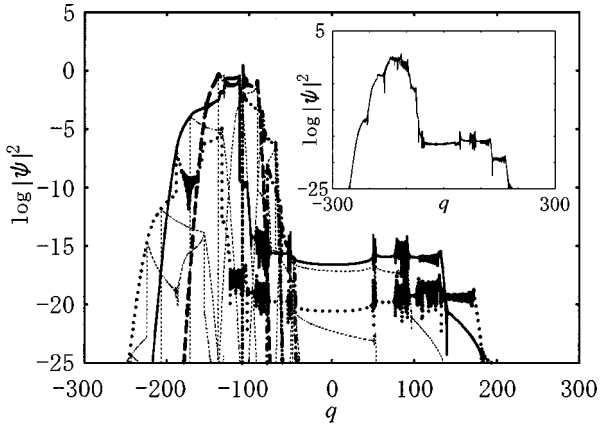

FIG. 5. The semiclassical wave function for ten time steps resolved into contributions from different generations. Each component corresponds to the branches with the same line styles in Fig. 2(a). The thin dashed lines represent those branches which are dominated, in each coordinate q, by some other branches. (Inset) The semiclassical wave function finally obtained by the superposition of these contributions.

shown in Fig. 1 is excellent. The origin of plateau-cliff structure is understood by resolving the superposed semiclassical function into contributions from individual generations. The plateau-cliff structure is created because each semiclassical component itself has a flat plateau accompanied by sharp drop and interference between branches forming the generation give rise to erratic oscillation on the plateau. Discontinuity of amplitude, as found in $q \approx -168, -207, -224$, etc. are caused by the Stokes phenomenon which is inevitable in the saddle point method, and is treated in an appropriate way [13].

It should be stressed that the most crucial step in our semiclassical analysis is to decode embedded information in MGS which reflects complex homoclinic entanglement. This means that emergence of the entanglement in complex phase space is an essential ingredient in our description. We think it is a quite general event in chaotic systems, and thus so-called plateau-cliff structure, which is typically observed pattern of tunneling in the presence of chaos [5], must appear as a manifestation of such complex structures. We can therefore expect that, whether energetic or dynamical, there is a common semiclassical mechanism of the tunneling phenomena in chaotic map systems, which should be attributed to the structure of entanglement, typically observed as MGS.

[1] M. Wilkinson, Physica D **21**, 341 (1986); **27**, 201 (1987).
[2] O. Bohigas, S. Tomsovic, and D. Ullmo, Phys. Rep. **223**, 43 (1993); S. Tomsovic and D. Ullmo, Phys. Rev. E **50**, 145 (1994).
[3] W. A. Lin and L. E. Ballentine, Phys. Rev. Lett. **65**, 2927 (1990).
[4] S. C. Creagh, in *Tunneling in Complex Systems*, edited by S. Tomsovic (World Scientific, Singapore, 1998), p. 35.
[5] A. Shudo and K. S. Ikeda, Physica D **115**, 234 (1998); Prog. Theor. Phys. Suppl. **139**, 246 (2000).
[6] S. D. Frischat and E. Doron, Phys. Rev. E **57**, 1421 (1999).
[7] W. H. Miller and T. F. Gorge, J. Chem. Phys. **56**, 5668 (1972); W. H. Miller, Adv. Chem. Phys. **25**, 69 (1974).
[8] S. C. Creagh and N. D. Whelan, Phys. Rev. Lett. **77**, 4975 (1996); **82**, 5237 (1999).
[9] K. Takahashi, A. Yoshimoto, and K. S. Ikeda (unpublished).
[10] V. G. Gelfreich, V. F. Lazutkin, C. Simo, and M. B. Tabanov, Int. J. Bifurcation Chaos Appl. Sci. Eng. **2**, 353 (1992).
[11] T. Onishi, A. Shudo, K. S. Ikeda, and K. Takahashi (unpublished).
[12] A. Shudo, Y. Ishii, and K. S. Ikeda (unpublished).
[13] A. Shudo and K. S. Ikeda, Phys. Rev. Lett. **76**, 4151 (1996).